# Biodegradation and antimicrobial properties of zinc oxide–polymer composite materials for urinary stent applications

coatings

MDPI

Article

# Biodegradation and Antimicrobial Properties of Zinc Oxide–Polymer Composite Materials for Urinary Stent Applications

**Chaitra Venkatesh [1,†], Marco Laurenti [2,†], Marina Bandeira [1,3], Eduardo Lanzagorta [1], Lorenzo Lucherini [2,4], Valentina Cauda [2,*] and Declan M. Devine [1]**

1 Material Research Institute, Athlone Institute of Technology, Athlone, N37 HD68 Co. Westmeath, Ireland; c.venkatesh@research.ait.ie (C.V.); m.bandeira@research.ait.ie (M.B.); e.lgarcia@research.ait.ie (E.L.); ddevine@ait.ie (D.M.D.)
2 Department of Applied Science and Technology, Politecnico di Torino, C.so Duca degli Abruzzi 24, 10129 Turin, Italy; marco.laurenti@polito.it (M.L.); lucherini.lorenzo@gmail.com (L.L.)
3 Rua Francisco Getúlio Vargas, Universidade de Caxias do Sul, 1130, Caxias do Sul 95070-560, RS, Brazil
4 Soil Mechanics Laboratory (LMS), École Polytechnique Fédérale de Lausanne (EPFL), Station 18, CH-1015 Lausanne, Switzerland
* Correspondence: valentina.cauda@polito.it; Tel.: +39-11-0907389
† These authors contributed equally to this work.

Received: 5 October 2020; Accepted: 18 October 2020; Published: 20 October 2020


**Abstract:** Research advancements in the field of urinary stents have mainly been in the selection of materials and coatings to address commonly faced problems of encrustation and bacterial adhesion. In this study, polylactic acid (PLA) and polypropylene (PP) were evaluated with zinc oxide (ZnO) coating to assess its ability to reduce or eliminate the problems of encrustation and bacteria adhesion. PLA and PP films were prepared via twin screw extrusion. ZnO microparticles were prepared using sol-gel hydrothermal synthesis. The as-prepared ZnO microparticles were combined in the form of a functional coating and deposited on both polymer substrates using a doctor blade technique. The ZnO-coated PP and PLA samples as well as their uncoated counterparts were characterized from the physicochemical standpoints, antibacterial and biodegradation properties. The results demonstrated that both the polymers preserved their mechanical and thermal properties after coating with ZnO, which showed a better adhesion on PLA than on PP. Moreover, the ZnO coating successfully enhanced the antibacterial properties with respect to bare PP/PLA substrates. All the samples were investigated after immersion in simulated body fluid and artificial urine. The ZnO layer was completely degraded following 21 days immersion in artificial urine irrespective of the substrate, with encrustations more evident in PP and ZnO-coated PP films than PLA and ZnO-coated PLA films. Overall, the addition of ZnO coating on PLA displayed better adhesion, antibacterial activity and delayed the deposition of encrustations in comparison to PP substrates.

**Keywords:** polylactic acid (PLA); polypropylene (PP); zinc oxide; antibacterial coatings; ureteral stents; bacteria biofilm; urine-derived encrustations

## 1. Introduction

Urinary stents are commonly used to drain retained urine after surgical procedures, in cases of urinary incontinence and in related issues to the urinary tract [1–3]. Although many improvements have been achieved so far, patients still face complications related to the insertion of urinary stents, especially when long-term usage is required. The main problems encountered in commercial urinary stents are friction, the release of substances, encrustation and bacterial adhesion that can cause adverse

effects to the patient, such as inflammation [1,4–6]. To date, work is still in progress on the development of a biocompatible, antimicrobial, antifouling and nonfrictional material potentially used for urinary stents to improve patients' quality of life by reducing the chances of postprocedure complications as well as to increase the lifetime of the stent [7–9].

Different materials have been employed to develop urinary stents. However, polymer-based materials are the most used due to their biocompatibility, biological inertness and low cost [7,10]. Moreover, several coatings technologies have been shown to improve biocompatibility, antimicrobial action and prevent encrustation, illustrating the potential of coatings to enhance the functionality of urinary stents [2,8,9,11] and even promoting the sustained delivery of pharmaceutically active compounds [12]. For example, antibiotics coatings were able to prevent biofilm formation and bacterial infections. However, many issues related to antibiotic resistance have been addressed, showing the loss of antimicrobial action after a few usages [8,13].

In this study, the performance of polylactic acid (PLA) and polypropylene (PP) as a material for urinary stents were evaluated. PLA is the most widely used aliphatic thermoplastic polymer. It is obtained from renewable agricultural resources such as starch from rice, corn, potatoes, beetroot, etc. and is used in various medical applications such as sutures, dermal fillers or stents [14]. PLA has been studied as a coating layer for antimicrobial applications by incorporation of nanoparticles such as silver [15], zinc oxide (ZnO) nanoparticles [16] or ZnO deposition on halloysite nanotubes and further incorporation into PLA [17]. PLA-ZnO nanocomposites have been produced by the method of melt compounding, and the resultant films were found to be amorphous and had antibacterial properties [18,19] and degradation process of the PLA was increased [20].

PP is a polymer from the family of polyolefins that has features such as low density, chemical inertness, and high melting temperature. Due to its high temperature resistance, it is used in various products in clinical environments [21]. It has been used for stenting in endoscopic dacryocystorhinostomy with successful and higher anatomic and functional efficacy [22,23]. Due to its excellent histocompatibility PP mesh has been studied as suitable stent material for airway strictures [24] and PP-silicone stent has been successfully evaluated for the treatment of benign esophageal strictures [25]. In order to enhance the properties of PP, different methodologies have been tested including reports by Zhao et al. who investigated the photodegradation resistance of PP to UV-irradiation by incorporation of ZnO and found significant improvements [26]. PP has been modified with ZnO to produce hybrid filter material and found to have high filtration efficiency [27]. Bojarska et al. investigated PP capillary membranes which were modified by ZnO nanowires. The use of plasma was found to improve the adhesion of ZnO nanowires on the PP membrane surface. Moreover, the resulting PP/ZnO membranes exhibited antibacterial properties against Gram-positive and Gram-negative bacteria [28].

This work aims to evaluate the use of ZnO as a novel coating material for the manufacturing of urinary stents. In particular, to achieve a material with superior antimicrobial property, both PLA and PP films were coated with a functional ZnO layer, as zinc oxide is well known for its antimicrobial action against both Gram-positive and Gram-negative bacteria [29,30]. Briefly, the mechanism of antimicrobial action involves the release of zinc ions, production of reactive oxygen species (ROS) and direct contact with the bacteria cell surface causing the rupture of the membrane and changes on the cell metabolism that can lead to cell death [31–34]. Thus, this research focused on the evaluation of the physical and mechanical properties, antimicrobial activity and adhesion of the zinc oxide coatings on PLA and PP substrates for urinary stents application. In particular, we show a different capability of these materials to react to artificial urine solution and another simulated physiological solution, which has a similar inorganic composition of the human plasma. The results indeed show that the behaviour of these ZnO-coated polymers can be efficiently modulated to get highly hydrophilic and biodegradable devices with further antimicrobial properties in the right urinary environment.

## 2. Materials and Methods

### 2.1. Preparation of PLA and PP Films

Polylactic acid (PLA) obtained from Corbion, PLA LX 175 (Total Corbian, Gorinchem, The Netherlands) and polypropylene (PP, Sigma Aldrich Ireland Ltd., Wicklow, Ireland) were used to produce the polymeric substrates. The PLA had a molecular weight ($M_w$) of 24,000 g/mol and PP was isostatic with average $M_w$ of ~250,000 g/mol. Both polymers were received in granular form.

Twin-screw extrusion was employed to process PLA and PP into films. Extrusion was performed by using an APV (Model MP19TC (35:1) APV Baker, Newcastle-underLyme, UK) twin-screw compounder with 19 mm diameter screws. The temperature profile was maintained (from die to feeder) at 200/190/180/170/160/110/50 °C. PLA was dried in the oven at 80 °C for 4 h. The dried PLA pellets were fed into the hopper of the extruder and extruded at a screw speed of 140 rpm. Extruded strands of the molten composite were then drawn through a three-roll calendar creating continuous films. Similarly, the PP pellets were processed by melt compounding under similar conditions for comparison. These films were used to punch out ASTM standard tensile test specimens by a physical punching process.

### 2.2. Synthesis of ZnO Microparticles

Zinc oxide microparticles were prepared via a sol-gel hydrothermal synthesis method as previously reported [35,36], using potassium hydroxide (KOH, Sigma Aldrich, Darmstadt, Germany) and zinc nitrate hexahydrate ($Zn(NO_3)_2{\cdot}6H_2O$, Sigma Aldrich) as precursors. All reagents were used as received. First, 5.58 g of potassium hydroxide and 14.8 g of zinc nitrate hexahydrate were dissolved separately in 100 mL of double-distilled water at room temperature. Afterwards, the zinc nitrate solution was added dropwise to the KOH solution under vigorous magnetic stirring conditions. The formed gel was treated at 70 °C for 4 h. Later, the precipitated ZnO powder was filtered from the basic solution and washed several times with demineralized water until pH neutralization and air dried in a muffle furnace at 60 °C overnight.

### 2.3. Deposition of ZnO Coating on Polymeric Substrates

Different methods were considered to coat PLA and PP substrates. First, a ZnO paste was prepared by adding zinc oxide powders in a 1:2 (*w*/*v*) ratio to a solution of acetic acid (1%, Sigma Aldrich), ethanol (67%, Sigma Aldrich) and water (33%). The paste was then stirred and sonicated to obtain a homogeneous dispersion of the particles. The prepared paste was deposited on the surface of both PP and PLA films using the doctor blade technique on a glass slide to obtain a uniform layer. Sodium hydroxide (Sigma Aldrich) and benzophenone (BP) (Sigma Aldrich) were also used for surface activation and grafting of the ZnO coatings to the polymer supports.

In this study three methods were employed:

1. For method 1, the coated PLA was thermally treated at 50 °C for 30 min and 60 °C for 15 min while coated PP films were treated at 70 °C for 15 min.
2. In method 2, ZnO paste was UV grafted onto the PLA substrate using the protocol developed by Shin et al. [37] with adaptations. For this, 20 mL of 10 wt.% acrylic acid aqueous solution was added to 20 mL of benzophenone 0.2 M and stirred under dark conditions. Then, ZnO paste containing 1 g of ZnO was added to the previous solution and stirred for 30 min in the absence of light. The final solution was poured in a glass petri dish containing the PLA films and exposed to UV light for five minutes at 40 W. After curing, samples were neutralized by immersion in a sodium bicarbonate (Sigma Aldrich) 0.1 M solution for 10 min, rinsed with distilled water and dried overnight at 40 °C.
3. In method 3, 1 g of ZnO powder was dispersed in 2 mL of ethanol and sonicated for 15 min. Different amounts of benzophenone 0.2 M ethanolic solution (0, 0.25 and 0.50 mL) were then

added to this solution and stirred until the solution became homogeneous. Then, PP and PLA were coated with ZnO + BP solution and exposed to UV light (0, 5 and 10 min), dried for 1 h at 37 °C and rinsed with water for removing excess reagents. All samples were dried overnight at 37 °C prior to analysis. For this method, PP was previously treated with a 0.1 M sodium hydroxide solution for 18 h for surface activation while PLA did not have any previous treatment.

Only the coatings produced using method 3 with 0.50 mL of BP and 5 min of UV treatment for PLA films and 0.50 mL of BP and no UV treatment for PP films showed good adhesion of the coatings (data not shown). Thus, only these set of samples (named ZnO@PP and ZnO@PLA) were fully characterized in this work.

### 2.4. Characterization Setup

#### 2.4.1. Physicochemical Characterization

The morphology and chemical composition of the samples were investigated by means of field-emission scanning electron microscopy (FESEM, Merlin Carl Zeiss AG, Oberkochen, Germany) coupled with an energy dispersive x-ray (EDX) detector for chemical composition analyses. Before FESEM imaging, the surface of the samples was coated with a 5 nm-thick Pt coating. The crystalline structure was investigated with X-ray diffraction (XRD) using a Panalytical X'Pert PRO diffractometer (Malvern Panalytical S.r.l., Milan, Italy) in Bragg–Brentano configuration and equipped with a Cu Kα monochromatic radiation (λ = 1.54059 Å) as X-ray source. Fourier transform infrared spectroscopy (FTIR) in attenuated total reflectance (ATR) mode was performed with a Nicolet 5700 FTIR spectrometer (ThermoFisher, Waltham, MA, USA) equipped with diamond crystal. The ATR-IR spectra were background subtracted and acquired with 2 $cm^{-1}$ resolution and 64 scans accumulation. Indexing of IR modes have been done according to Socrates [38].

Mechanical properties of the PLA and PP films were characterized by tensile tests, probing each different blend. Tensile testing was carried out on a Lloyd Lr10k tensometer (Ametek ltd, West Sussex, UK) using a 2.5 kN load cell on ASTM standard test specimens at a strain rate of 50 mm/min. Data was recorded using NexygenTM software (Ametek Ltd.). The tensile tests were carried out in adherence to ASTM D 882. Ten individual test specimens were analysed per group and before testing, the thickness of each sample was measured. The percentage strain at maximum load, stress at maximum load, stiffness, and Young's modulus of each sample were recorded.

The surface wettability of the composites was assessed using First Ten Angstroms' FTA32 goniometer (FTA Europe, Cambridge, UK). In this test, the sessile drop contact angle technique was utilized with distilled water as the probe liquid. Five measurements at various places on the films were taken.

Differential scanning calorimetry (DSC) was carried out using a DSC 2920 modulated DSC (TA Instruments, New Castle, DE, USA) with a nitrogen flow rate of 20 mL/min to prevent oxidation. Calibration of the instrument was performed using indium as standard. Test specimens weighing between 8 mg and 12 mg were measured on Sartorius scales (MC 210 P, Sartorius Lab Instruments GmbH & Co. KG, Goettingen, Germany), capable of being read to five decimal places. Samples were crimped in nonperforated aluminium pans, with an empty crimped aluminium pan used as the reference. The thermal history was removed by heating samples from 20 to 220 °C at the rate of 30 °C/min and then held isothermally at 220 °C for 10 min. The samples were then cooled down from 220 to 20 °C at 30 °C/min. Finally, the thermal properties of the samples were recorded by heating the samples from 20 to 220 °C at the rate of 10 °C/min, glass transition temperature, and melting temperature of each sample were recorded.

#### 2.4.2. Biodegradation Essays

Simulated body fluid (SBF) was prepared according to the method described by Kokubo and Takadama [39] with a final pH of 7.45. ZnO-coated PLA and PP films were then placed in the SBF

solution in a water bath at 36.5 ± 1 °C. The SBF solution was replaced every two days and the adhesion of the films in SBF solution was monitored for seven days.

The artificial urine was prepared following the protocol described by Sarangapani et al. [40]. The solution was constituted basically by salts, urea (25 $g \cdot L^{-1}$) and creatinine (1.10 $g \cdot L^{-1}$). The final pH of the solution was 5.7. ZnO-coated films were placed in the artificial urine solution, which was kept at 36.5 ± 1 °C, and monitored for 21 days regarding the adhesion and appearance of encrustation. Uncoated PLA and PP films were also placed in artificial urine for the same soaking time and used as control samples.

#### 2.4.3. Antibacterial Tests

The antimicrobial tests were performed using Staphylococcus aureus ATCC25923 (*S. aureus*) and Escherichia coli ATCC25922 (*E. coli*), tryptone soy broth (TSB, Neogen) and resazurin (Sigma Aldrich). *S. aureus* and *E. coli* were cultured and grown in an exponential phase in TSB medium at 37 °C. Bacterial cell viability when exposed to different polymer films was analysed in a 12-well plate according to the resazurin cell viability assay. Resazurin indicates cell viability by changing the solution colour from blue to pink when it is chemically reduced to resofurin due to the aerobic respiration that occurs with cell growth. Thus, the reduction of the dye is proportional to the viable cells present in the solution. Overnight cultures of the two bacteria strains were diluted to a concentration of approximately $1.0 \times 10^4$ colony formation unit per millilitre ($CFU \cdot mL^{-1}$). Then, 500 µL of TSB and 25 µL of the diluted bacteria were added in each well. After this procedure, coated (10 mm × 10 mm) and noncoated polymer films were placed in the respective wells. A negative control without bacteria (500 µL of TSB) and positive control with live cells (500 µL of TSB and 25 µL of diluted bacteria solution) were also included in each plate. After overnight incubation at 37 °C, 75 µL of resazurin was added in every well, mixed thoroughly and incubated for 2 h at 37 °C under dark conditions. Then, the colour change of the solution and, consequently, the cell viability was evaluated by absorbance measurement at 600 nm in an ultraviolet-visible (UV-Vis) plate reader (Jenway 6300, Staffordshire, UK). The experiment was performed in triplicate and repeated independently three times.

#### 2.4.4. Statistical Analysis

Statistical analysis of the tensile test results, DSC measurements and the surface wettability measurements were carried out using general linear model (GLM) of two-way ANOVA in Minitab 17 Statistical Software (Minitab Ltd., Coventry, UK). All the values were considered at a 95% confidence interval, and $p$-values are considered significant when $p \leq 0.05$.

## 3. Results and Discussion

### *3.1. Morphological, Structural and Chemical Characterization*

Figures 1–3 show the FESEM images and EDX spectra of ZnO-coated PLA and PP substrates (ZnO@PLA and ZnO@PP). It can be observed that ZnO microparticles showing a flower-like morphology (Figure 2) have been successfully deposited atop of both the polymer surface types. Their presence is further corroborated by the detection of Zn traces by EDX analyses. The covering of the PLA substrate is superior with respect to the PP one. This is visible from the comparison of the FESEM images and of the semiquantitative analysis obtained by EDX spectroscopy. Actually, the Zn at.% changes from 31.90% for PLA support to 9.76% for PP, suggesting that ZnO is more abundant on PLA than on PP films.

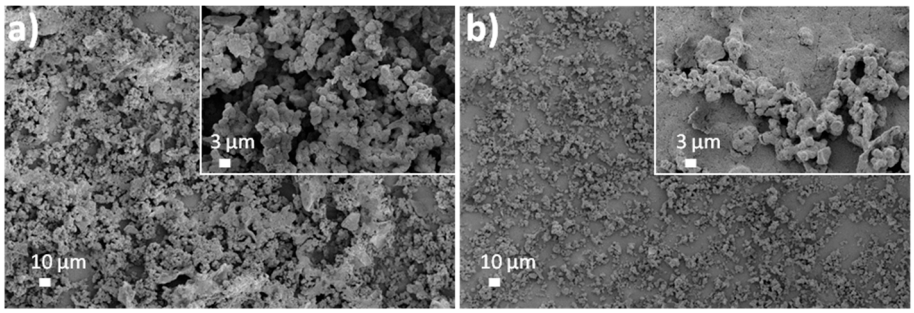


**Figure 1.** Field-emission scanning electron microscope (FESEM) images of ZnO microparticle coatings deposited on (**a**) polylactic acid (PLA) and (**b**) polypropylene (PP) polymeric supports.

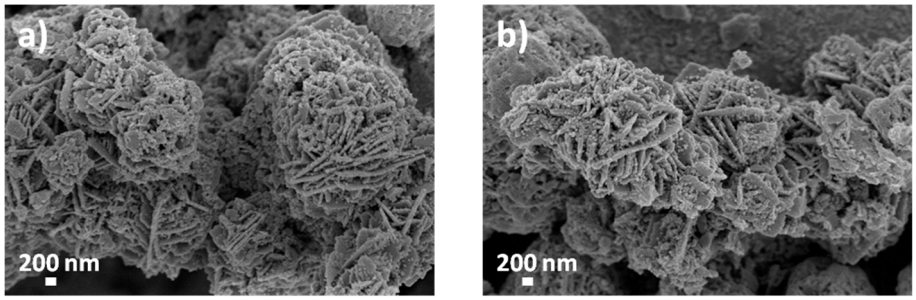


**Figure 2.** FESEM images showing the flower-like morphology of ZnO microparticle coatings deposited on (**a**) PLA and (**b**) PP polymeric supports.

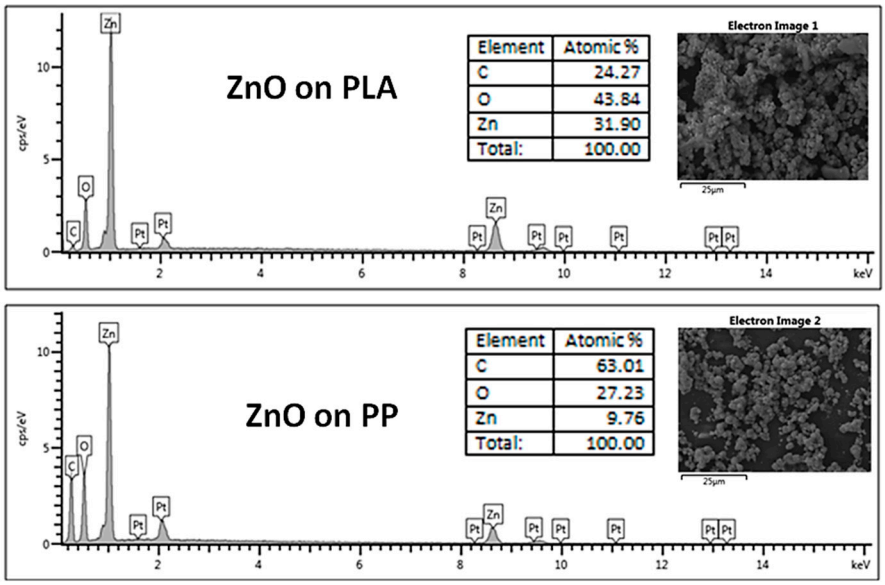


**Figure 3.** Energy dispersive X-ray (EDX) spectra of ZnO-coated PLA and PP supports.

Independently of the polymer, the presence of the ZnO coating after the fabrication process was confirmed also by the detection of the diffraction peaks belonging to wurtzite ZnO phase (Figure 4). The main ones are positioned at 31.8°, 34.4° and 36.2°, and are ascribed to (100), (002) and (101) crystallographic planes according to the Joint Committee on Powder Diffraction Standards—International Centre for Diffraction Data (JCPDS-ICDD) database (Card No. 89-1397). Other minor reflections coming from additional crystal planes are also visible at higher 2θ angles.

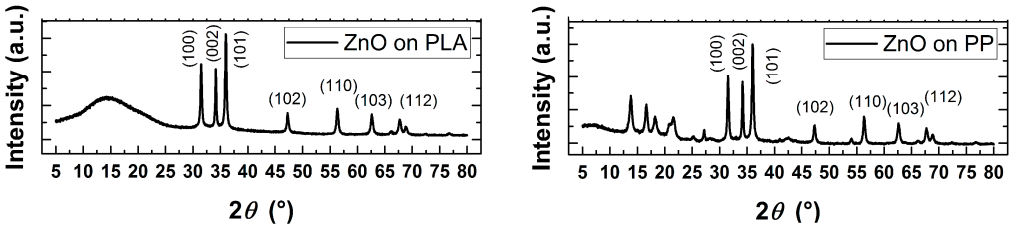


**Figure 4.** X-ray diffraction (XRD) pattern of sample ZnO@PLA and ZnO@PP.

Figure 5 shows the ATR-IR spectra for uncoated PLA and PP substrates as well as from the corresponding samples coated with ZnO microparticle film. The main IR modes are in the range 3000–2900 $cm^{-1}$ and near 1450 $cm^{-1}$ (both related to the C–H stretching/bending vibrations), at about 1750 $cm^{-1}$ (C=O stretching vibration), in the range 1200–1150 $cm^{-1}$ (C–O symm. stretch.) and three bands in the range 1130–1040 $cm^{-1}$ due to C–O–C symmetric stretching. These prominent modes of the spectrum are the characteristic peaks of PLA and PP [14,26,27]. When the ZnO microparticle coating is present, it is possible to observe a general reduction in intensity of the bands related to the polymeric materials underneath the ZnO materials. This effect is due to the micrometer thickness of the ZnO layer coating (more or less uniformly) the polymer. An additional broad band corresponding to H–O–H vibration of the ZnO hydrophilic surface is noticed in the range 3500–3000 $cm^{-1}$ for both kinds of ZnO-coated polymers. The presence of the ZnO coating is further confirmed by the presence of a broad band in the range 950–850 $cm^{-1}$ and due to Zn–OH mode. Similar presence of clear peak in the range 400–700 $cm^{-1}$ in PP/ZnO spectrum and absence in PP spectrum was observed in the study of ZnO nanowire growth via plasma activation by Bojarska et al. which could indicate the presence of zinc oxide [28].

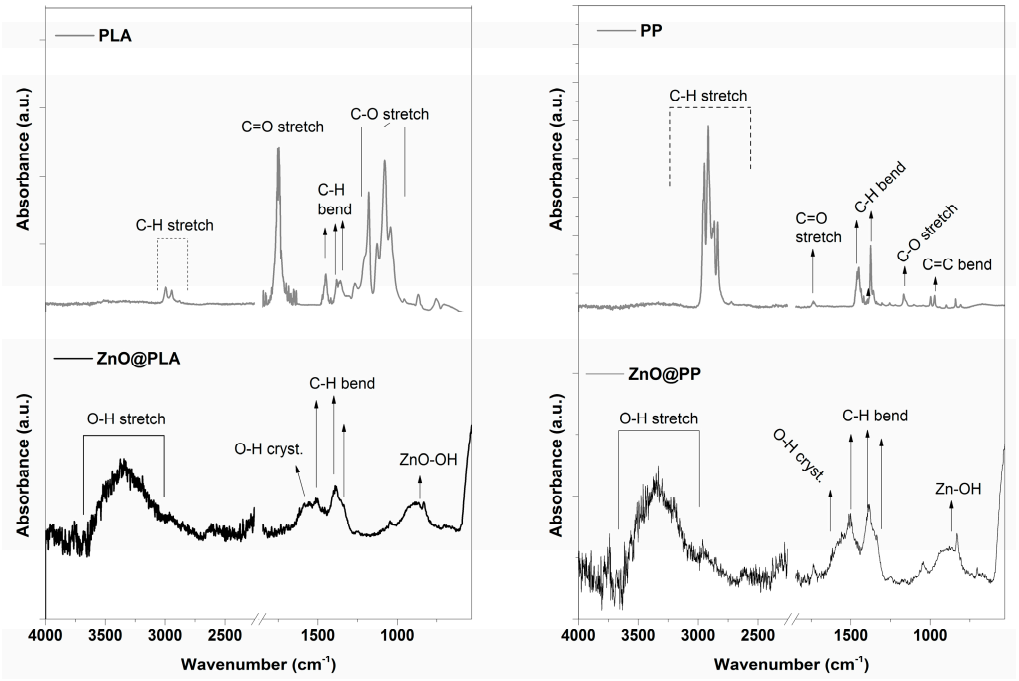


**Figure 5.** ATR-IR spectra of PLA and PP supports, with or without the presence of the ZnO coating.

### *3.2. Tensile Testing*

The mechanical behaviour of PLA and PP polymers are analysed with and without the presence of the ZnO coating. The graphical representation of the mechanical properties are shown in Figure 6. In case of PLA and ZnO@PLA samples, no significant difference in the tensile strength, elongation at break, stiffness or Young's modulus ($p \geq 0.05$) are observed. Similar results are obtained for PP and

ZnO@PP samples. This could be because the ZnO particles film is deposited on the polymer surface, which does not have any impact on the bulk polymer properties. However, various studies have shown a significant difference in mechanical properties when ZnO nanoparticles (NPs) are encapsulated into the polymer matrix [17,18,41–43].

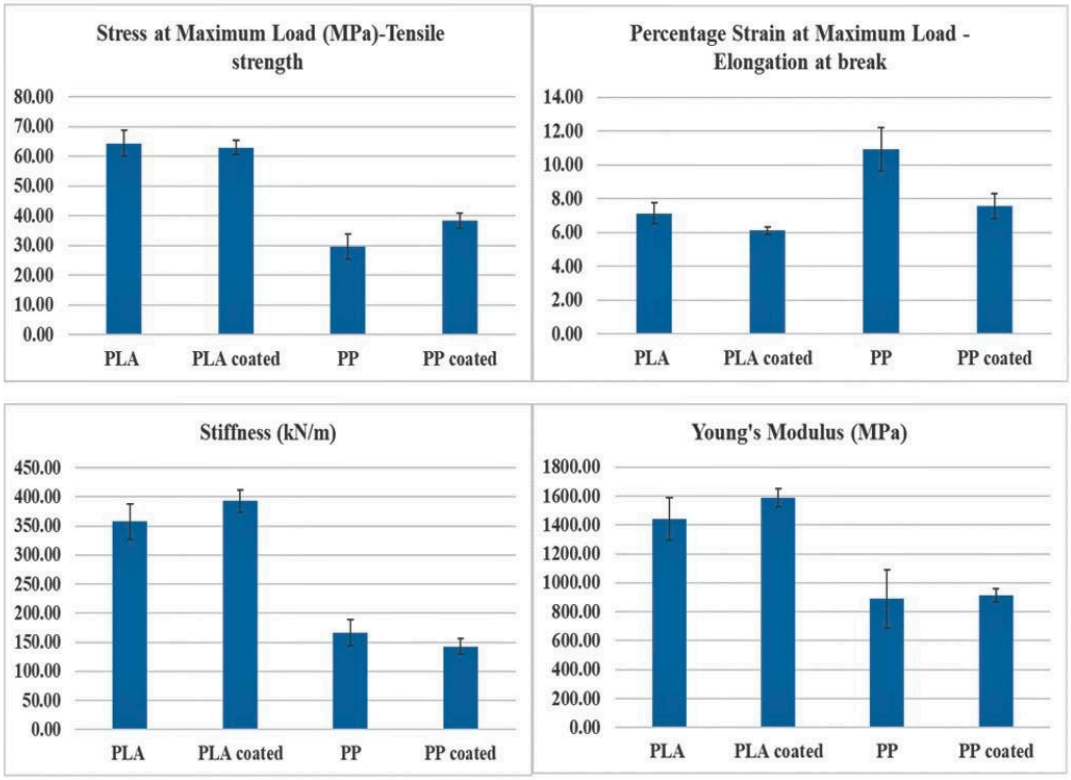


**Figure 6.** Graphical representation of the mechanical properties of the polymers with and without ZnO coating. There is no significant difference between the coated samples (ZnO@PLA ZnO@PP) and their uncoated counterpart samples.

### *3.3. Surface Wettability*

The surface wettability properties of all the coated and noncoated samples are shown in Figure 7. It was observed that there is a significant decrease in the contact angle of ZnO@PLA and ZnO@PP samples ($p = 1 \times 10^{-3}$) when compared to bare PLA and PP substrates. The photomicrographs of the uncoated PLA surface has a contact angle of 66°, whereas a contact angle of 24.07° is achieved for the sample ZnO@PLA. The images of the uncoated PP has a contact angle of 90.62°, and ZnO@PP has a contact angle of 44.55°. With PP being hydrophobic and PLA being relatively hydrophobic, these results indicate that the presence of the ZnO coating increased the hydrophilicity of the surface. A similar reduction in contact angle values was observed when PLA films were surface-modified and bulk-modified by plasma polymerization/sputtering technique, where glycerol and ethylene glycol were used as additives [15]. In another work, PP film was treated by plasma discharge in order to enhance the surface wettability of PP and improve the adhesion of ZnO NPs [27].

### *3.4. Differential Scanning Calorimetry (DSC)*

The thermal characteristics of the samples were analysed by DSC. The thermographs of the PLA, ZnO@PLA, PP and ZnO@PP samples are as shown in Figure 8. From the analysis of the thermographs, there is no evident difference between the coated and noncoated samples. However, in a study by Pantani et al. [18] the cold crystallization and melting temperature increased as ZnO NPs were incorporated into the PLA matrix by twin screw extrusion [18]. This confirms that the surface ZnO

coating of our work did not affect the bulk properties of the considered polymers, corroborating with the tensile test results.

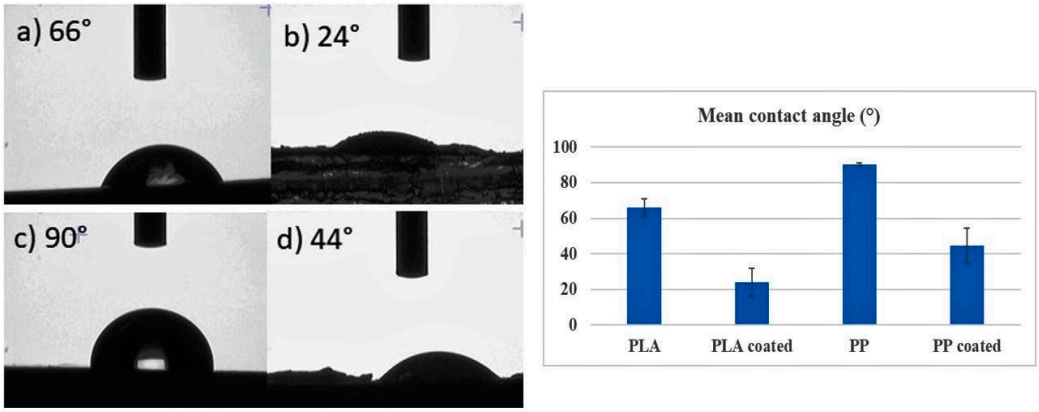


**Figure 7.** Surface wettability properties of the polymers with and without ZnO coating. With a *p*-value of 0.001, there is a significant decrease in the contact angle of ZnO@PLA and ZnO@PP when compared to the uncoated PLA and PP films. Water droplet on the surface of (**a**) PLA film, (**b**) ZnO@PLA, (**c**) PP film, and (**d**) ZnO@PP.

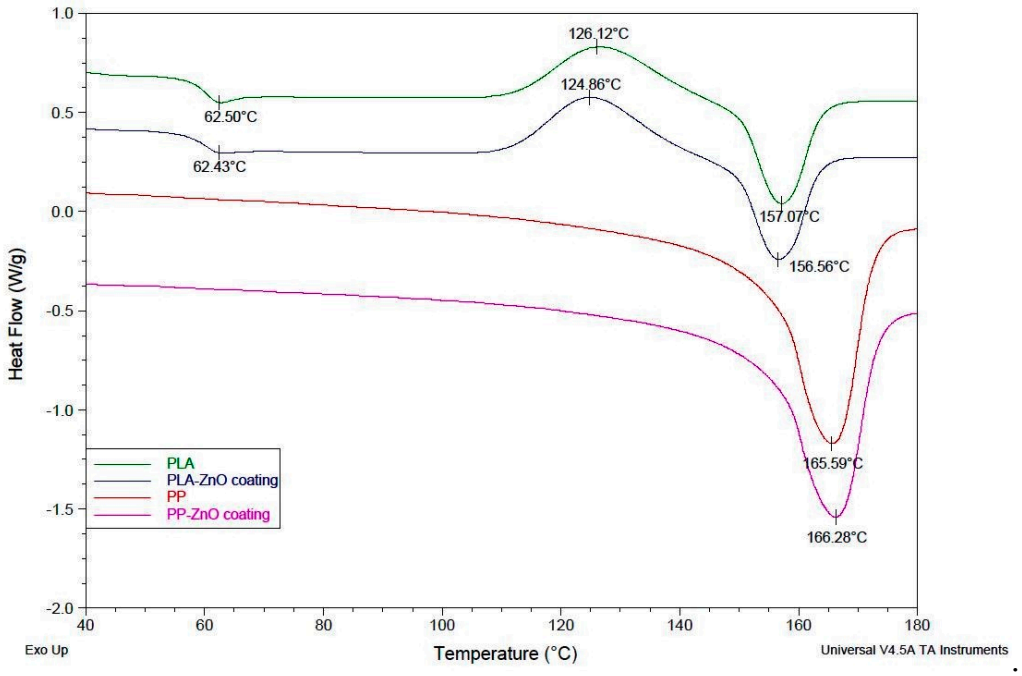


**Figure 8.** DSC thermographs of the PLA, ZnO@PLA, PP and ZnO@PP coated samples. No significant difference was observed between the coated and uncoated samples considering a *p*-value < 0.05.

### *3.5. Evaluation of the Biodegradation Properties in Biological Fluids*

#### 3.5.1. Simulated Body Fluid (SBF)

ZnO@PLA and ZnO@PP samples were immersed in simulated body fluid (SBF) solution to test the adhesion of the ZnO coating to the polymer substrate. Figure 9 shows the pictures of ZnO@PLA and ZnO@PP samples after immersion in this solution for up to seven days. In the case of the PP substrate, the ZnO coating showed a considerable detachment after 2 h in contact with the SBF solution. However, no major changes occurred from 2 h to seven days. Interestingly, no significant alterations

were observed for ZnO@PLA samples over time, which indicates a higher adhesion of the ZnO coating to the PLA substrate in comparison to the PP one and well agrees with the results shown in Figure 1.

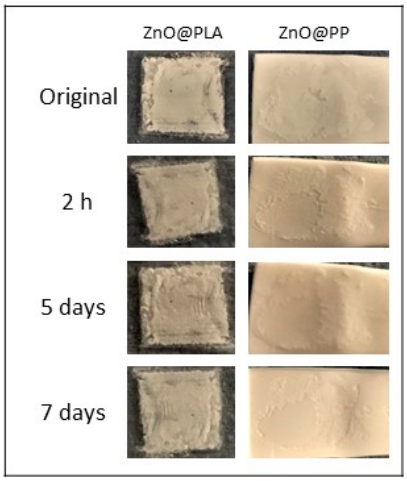


**Figure 9.** ZnO@PLA and ZnO@PP samples after different time intervals in SBF solution.

FESEM images reported in Figure 10a,c highlights that no visible changes in the morphology of the samples are present. The ZnO coating did not detach completely from the polymer supports and the flower-like ZnO microparticles preserve the original morphology. The presence of the ZnO coating is further confirmed by EDX measurements (Figure 10b,d). The compositional analyses also reveal the presence of P, Ca, Cl and Na, which are due to the prolonged contact of the samples with SBF solution. In particular, the abundance of Ca (around 1.9 at.%) and P (around 2–3 at.%) with respect to the other elements suggests the formation/precipitation of calcium phosphate compounds. This aspect is further supported by the IR spectroscopy results discussed in the following.

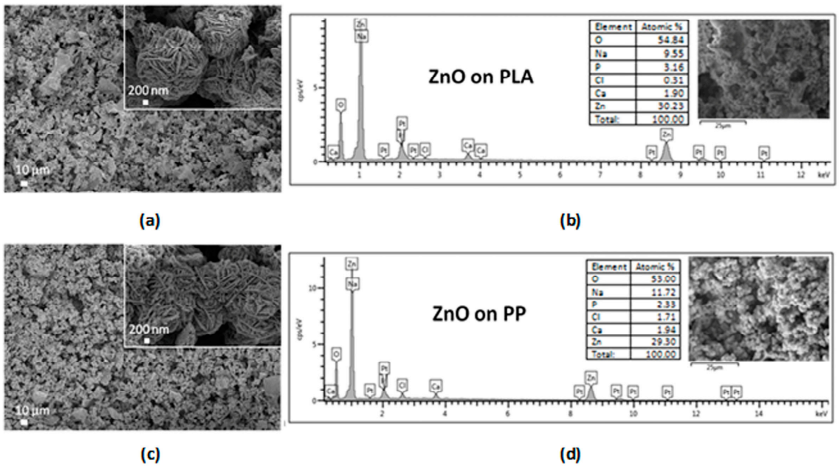


**Figure 10.** ZnO-coated PLA and PP supports soaked in SBF for 14 days: (**a**,**c**) FESEM images and (**b**,**d**) EDX spectra.

Figure 11 shows the IR spectra acquired after soaking all the sample typologies in SBF for 14 days. Panels a and b refer to the polymer substrates (PP and PLA) while panels c and d show the IR spectra acquired on ZnO@PLA and ZnO@PP samples, respectively. Considering the PLA and PP substrates, no changes are visible when compared to nonsoaked samples. This is likely related to the hydrophobic nature of the uncoated substrates. However, in the presence of the ZnO coating, a relatively intense band in the range 1100–1000 $cm^{-1}$ is observed due to the phosphate ($PO_4^{3-}$) vibration modes (Figure 11c,d). This is due to the interaction between the ZnO surface and phosphate

groups present in SBF solution, which favours the formation of zinc phosphate and calcium phosphate compounds [44,45]. This aspect was also underlined by the corresponding EDX results of Figure 10. This indicates that the presence of the ZnO coating would allow for a more reactive surface able to induce the precipitation of an apatite-like functional layer. In general, an increase of the OH band intensity in the range 3500–3000 $cm^{-1}$ is observed, irrespectively of the presence of ZnO and due to the adsorption of water after the prolonged contact with SBF solution.

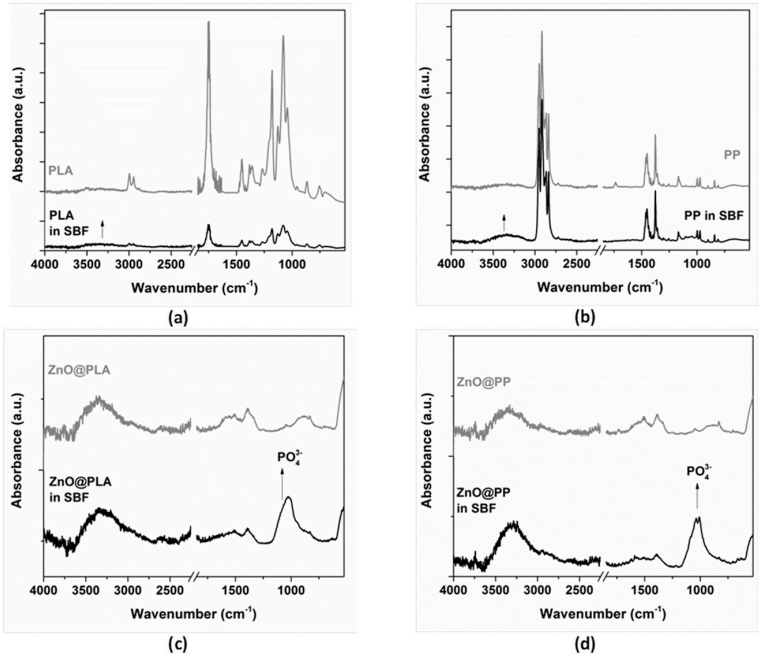


**Figure 11.** ATR-IR spectra of the samples after soaking in SBF for 14 days: (**a**) only PLA; (**b**) only PP; (**c**) ZnO@PLA; (**d**) ZnO@PP.

The XRD patterns of Figure 12a still show the presence of diffraction peaks belonging to wurtzite ZnO phase (indicated by arrows) and further witness the presence of the ZnO coating at the end of the biodegradation experiment in SBF.

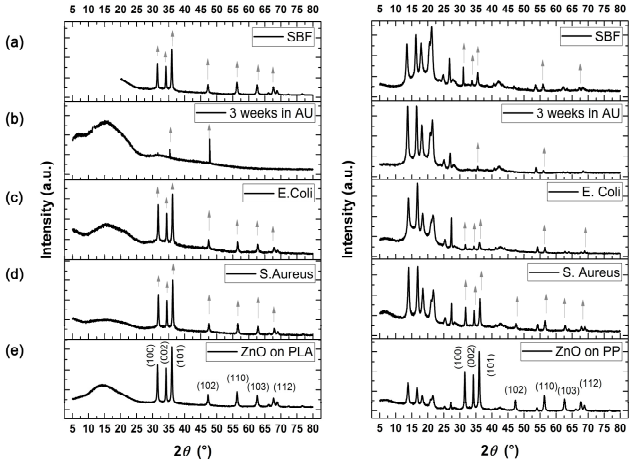


**Figure 12.** XRD pattern of samples ZnO@PLA and ZnO@PP: (**a**) after soaking in simulated body fluid solution for 14 days; (**b**) after immersion in artificial urine for 21 days; (**c**,**d**) at the end of the antimicrobial tests. XRD pattern of ZnO@PP and ZnO@PLA samples are also shown as reference in panel (**e**). Arrows indicate reflections coming from wurtzite ZnO phase.

### 3.5.2. Artificial Urine

When testing the coated polymer samples in artificial urine, a strikingly different behaviour was observed if compared to the SBF solution. As seen in Figure 13, ZnO@PLA samples show a considerable detachment of the ZnO layer after two days of immersion in artificial urine and a complete dissolution was observed after five days. Although the ZnO coatings on the PP supports are less uniform than on PLA, a slower dissolution was noticed when in contact with artificial urine. This might be related to the higher hydrophobicity of PP coated films that interact less with the solution in comparison to PLA films, as seen from the surface wettability analysis discussed in Section 3.3. Independently of the polymeric support, it can be noticed that the ZnO coating dissolved and/or detached faster in artificial urine than in SBF solution. This interesting feature can actually witness the fair tunability of our coated polymers, which selectively react differently upon the medium where they are immersed.

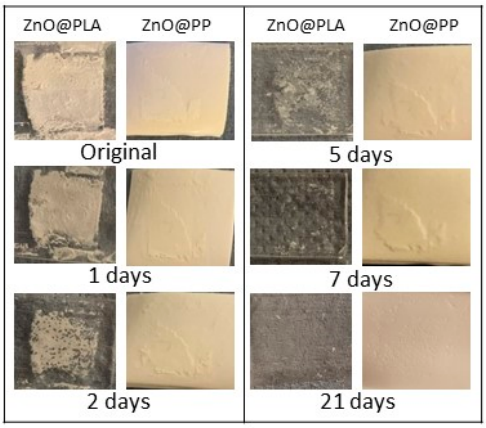


**Figure 13.** ZnO@PLA and ZnO@PP samples after different time intervals in artificial urine solution.

The biodegradation behaviour of ZnO@PLA and ZnO@PP samples was also evaluated in artificial urine solution for long time periods (21 days). Similarly, uncoated PLA and PP substrates were tested in the same experimental conditions, in order to evaluate any ability of ZnO to prevent the formation of encrustations in an artificial urine environment. If the uncoated PP and PLA supports are considered, the presence of precipitates with different morphologies and shapes can be observed (Figures 14 and 15): tabular-acicular surfaces, sheetlike, globular and spongelike structures are visible. In the case of the PP support (Figure 14), various type of encrustations can be found and in a more abundant way with respect to the PLA support (Figure 15).

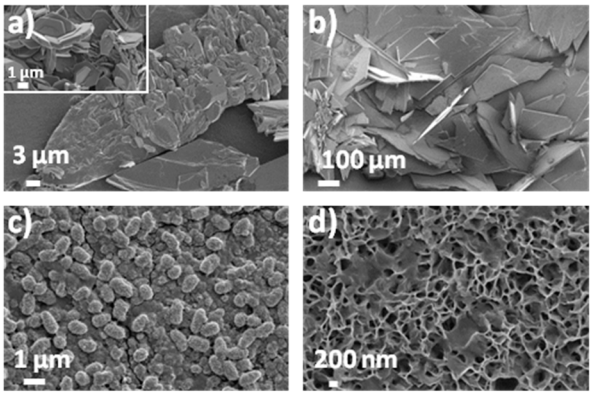


**Figure 14.** (**a**,**b**) FESEM images showing the formation of calcium phosphates precipitates and encrustations after immersion of PP support into artificial urine for 21 days. (**c**,**d**) Globular-shaped and spongelike morphology of hydroxyapatite precipitates.

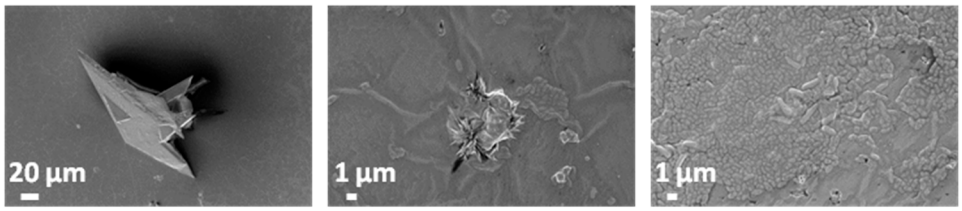


**Figure 15.** FESEM images of PLA support after immersion in artificial urine for 21 days.

By considering the morphology and the corresponding chemical composition summarized in Figures 16 and 17, calcium phosphate precipitates (Ca/P ratio around 0.9–1) are found for both the samples' types (Figure 14a,b and Figure 15) corresponding to brushite ($CaHPO_4{\cdot}2H_2O$) or hydroxyapatite $Ca_{10}(PO_4)_6(OH)_2$, the latter showing globular-shaped and spongelike morphology (Figure 14c,d) are detected only in the case of the PP support. For both PP and PLA supports, some traces of sodium chloride and potassium chloride are also present and due to the contact of the samples with artificial urine solution, while the presence of struvite $(NH_4)MgPO_4{\cdot}6H_2O$, corresponding to the crystalline prismatic deposits is also recognized (see the central Table in Figure 16). In Figure 15 (left panel), corresponding to the surface of the PLA sample, the typical crystalline structure of calcium oxalate $Ca(COO)_2$ is observed.

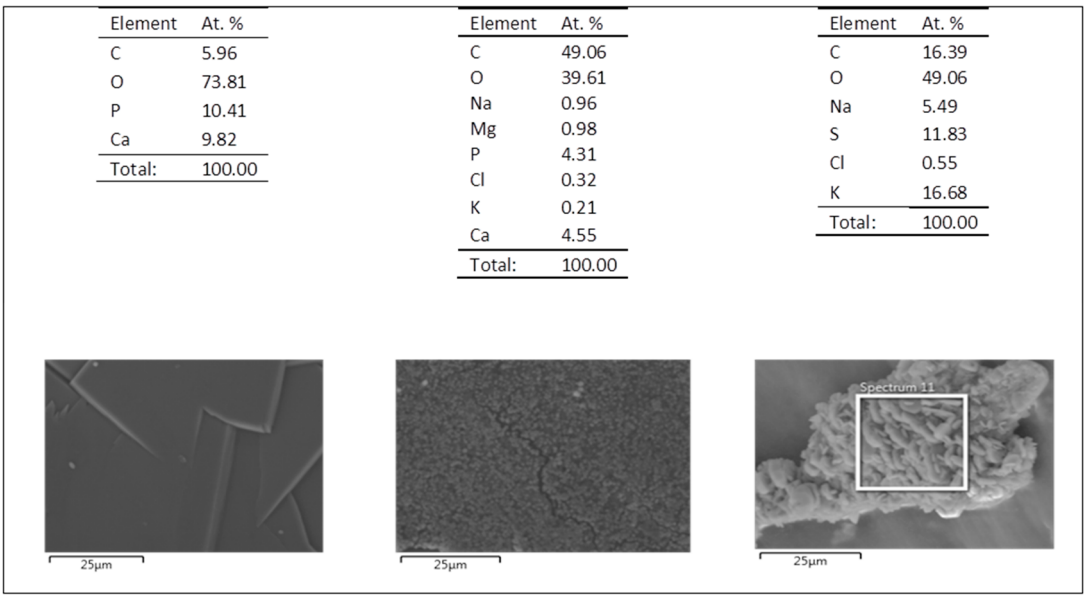


**Figure 16.** Chemical composition of three different precipitates formed at the surface of PP support after immersion in artificial urine for 21 days.

Differently from the previous case of SBF, the immersion of the ZnO-coated polymer substrates in artificial urine for 21 days negatively affected the ZnO morphology. A strong dissolution of the ZnO coating was observed through the corresponding FESEM images of Figures 18 and 19. There is an absence of the typical flowerlike microparticle morphology previously shown in Figure 1. The ZnO degradation is further supported by EDX analyses reported in Figures 20 and 21, showing small Zn traces in the case of sample ZnO@PP, while the amount of Zn is negligible for sample ZnO@PLA. Despite the degradation of the ZnO coating, a reduced amount of precipitates is observed for the ZnO@PLA support (Figure 19) with respect to the uncoated PLA counterpart. On the other hand, the presence of ZnO seems to not prevent the formation of encrustations in the case of the PP substrate (Figure 18), which could be related to the low level of ZnO coated onto the surface as observed in EDX. In particular, globular structures (peculiar of hydroxyapatite $Ca_{10}(PO_4)_6(OH)_2$), prismatic crystals of struvite ($(NH_4)MgPO_4{\cdot}6H_2O$) or brushite ($CaHPO_4{\cdot}2H_2O$) and layered sheetlike structures are

observed on ZnO@PP sample, while similar prismatic needlelike structures of struvite or brushite are found at the surface of sample ZnO@PLA. Furthermore, and similar to the previous case, the presence of sodium chloride (NaCl) and potassium chloride (KCl) is noticed also for the ZnO-coated polymers and due to the prolonged interaction of the samples with artificial urine solution.

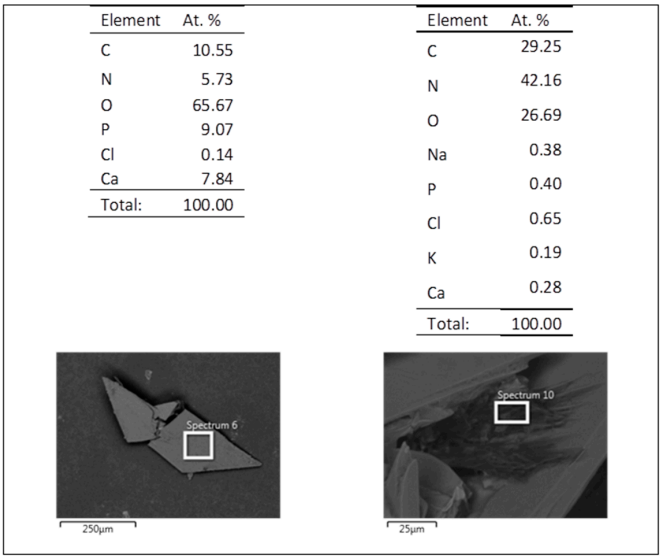


**Figure 17.** Chemical composition of three different precipitates formed at the surface of PLA support after immersion in artificial urine for 21 days.

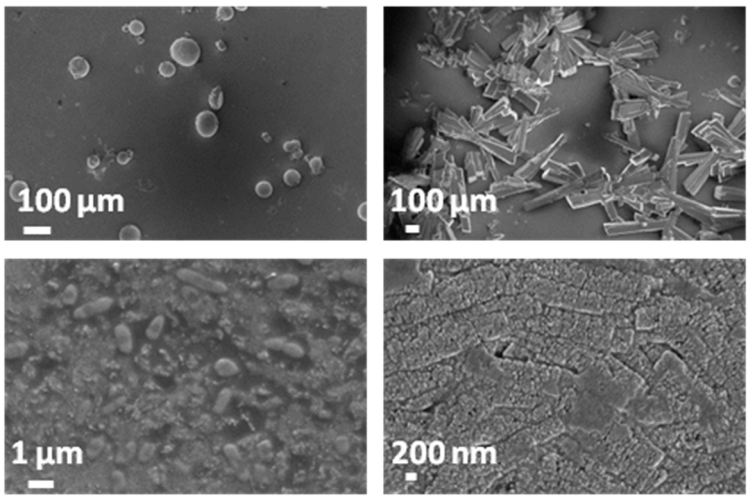


**Figure 18.** FESEM images of ZnO@PP sample after 21 days in artificial urine.

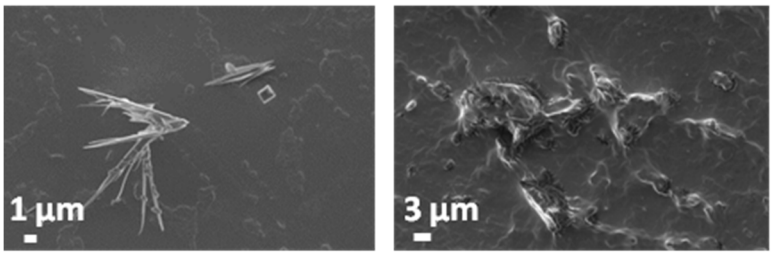


**Figure 19.** FESEM of ZnO@PLA sample after 21 days in artificial urine.

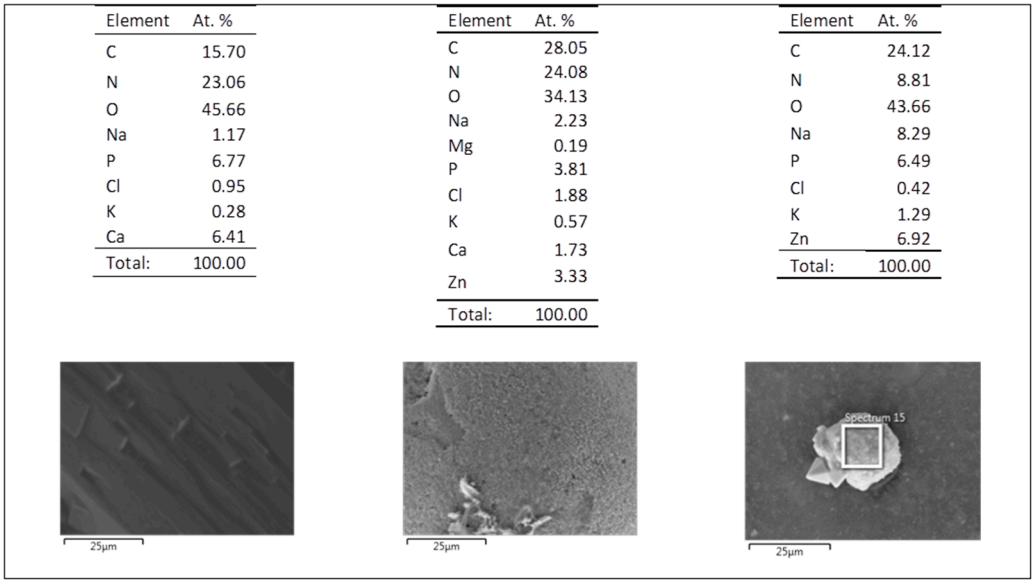


**Figure 20.** Chemical composition of three different precipitates formed at the surface of ZnO@PP sample after immersion in artificial urine for 21 days.

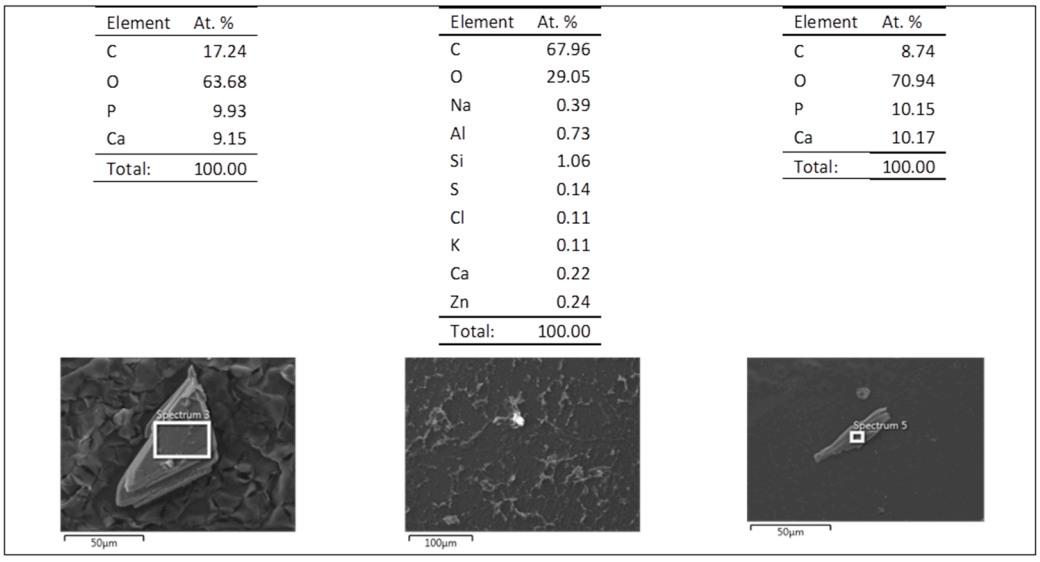


**Figure 21.** Chemical composition of three different precipitates formed at the surface of ZnO@PLA sample after immersion in artificial urine for 21 days.

Figure 12b shows the XRD pattern of ZnO@PLA and ZnO@PP substrates after the immersion in artificial urine for 21 days. In this case, the diffraction contribution coming from the ZnO microparticle film mostly disappear, with the (101) and (110) diffraction peaks being only slightly detectable. This aspect confirms the partial rather than complete degradation of the ZnO coating at the end of the experiment, as observed from FESEM analyses described previously.

ATR-IR analyses have been performed after soaking the sample in artificial urine for 21 days (Figure 22). Apart from the peaks characteristics of the polymer substrates, a strong change in the shape of the IR absorption band of 3500–3000 $cm^{-1}$ region is visible, and independent of the kind of polymer. In all the samples except ZnO@PLA, the presence of three distinct IR bands at 3218, 3331 and 3440 $cm^{-1}$ is noticed and confirms the formation of precipitates (mainly calcium phosphate compounds), as mentioned previously. These are due to stretching modes of vibration of water of crystallization as also to the N–H secondary stretching mode derived from urea. Additional IR modes

due to water of crystallization and N–H bending mode in the range 1670–1610 $cm^{-1}$ are detected as well. Such additional IR bands are barely detectable in sample ZnO@PLA and it confirms a reduced formation of encrustations and precipitates, as previously observed from the corresponding FESEM analyses. On the contrary, sample ZnO@PP shows additional IR bands with respect to the nonsoaked PP sample: the phosphate band in the 1100–1040 $cm^{-1}$ range and at 938 $cm^{-1}$, carbonate ($CO_2^{3-}$) bands in the range 1496–1434 $cm^{-1}$ and stretching mode of P–OH at around 866 $cm^{-1}$ [46].

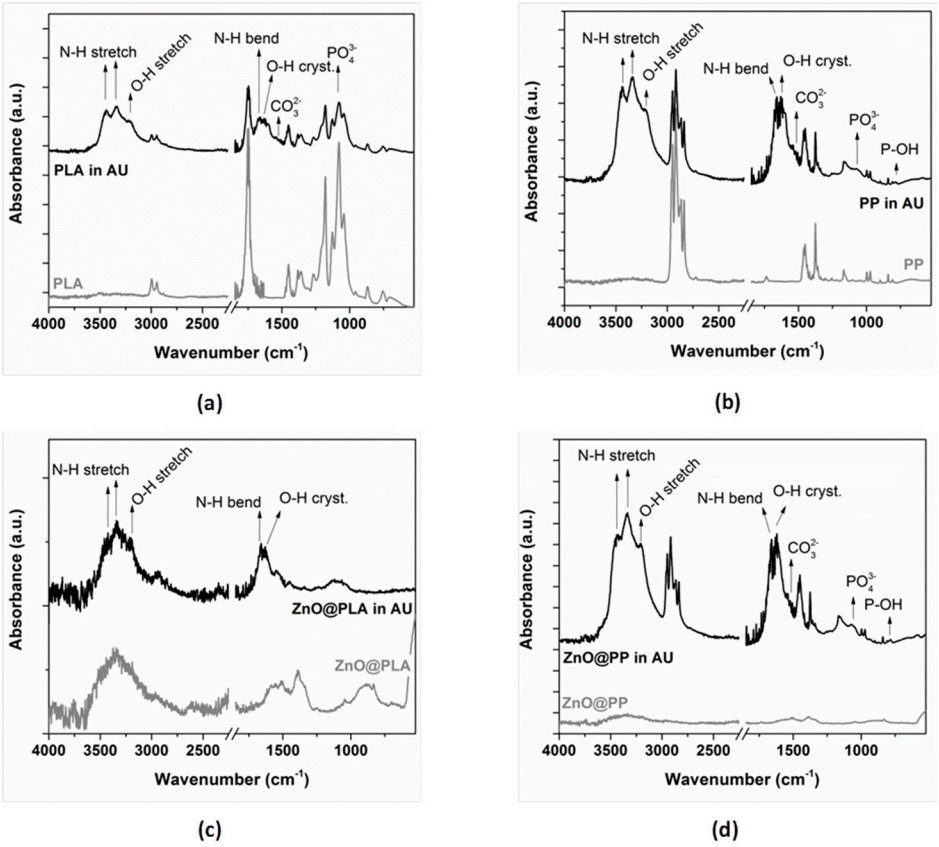


**Figure 22.** ATR-IR spectra of the samples after immersion in artificial urine for 21 days: (**a**) only PLA; (**b**) only PP; (**c**) ZnO@PLA; (**d**) ZnO@PP.

The strong degradation of the ZnO coating can be due to the acidic environment conditions of artificial urine, which induced ZnO dissolution. Actually, it is known that ZnO becomes more soluble as the pH of the solution decreases and dissolution increases significantly in pH values below 6.0 [47,48]. Thus, the different behaviours of the ZnO coating in both solutions and the faster dissolution of ZnO in artificial urine is probably related to its more acidic nature (pH 5.7) in comparison to the SBF solution (pH 7.45).

Another main issue related to urinary stents is the deposition of salts on the stent surface that can cause the blockage of liquid, inflammation and other complications [2,49]. In this study, encrustation was observed only after three weeks of immersion in artificial urine for ZnO-coated samples and two weeks for noncoated polymer supports. Hence, it can be concluded that the addition of the ZnO coating to both PLA and PP supports can be useful in preventing or at least delaying the deposition of encrustations.

### *3.6. Antimicrobial Tests*

Bacteria cell viability was evaluated on a Gram-negative strain (*E. coli*) and a Gram-positive strain (*S. aureus*). The bacteria strains were incubated in the presence of noncoated PLA and PP films, and ZnO-coated PLA and PP films. Figure 23 shows the average growth percentages of each strain when incubated with the coated and noncoated films, considering the positive control as the reference

for 100% of cell viability, as it was incubated without the presence of any polymer. Cell viability shows a clear reduction when incubated in the presence of ZnO-coated films. In *E. coli*, incubation with noncoated PLA and PP reached 96% viability, while for the incubation with ZnO@PLA and ZnO@PP samples, the viability was reduced to 70% and 71% respectively. Similarly, *S. aureus* achieved 96% and 91% viability with PLA and PP, respectively, but it reached only 67% with ZnO@PLA and 66% with ZnO@PP. With a 95% confidence interval, it was concluded that there is an important difference in cell viability mean values between the ZnO-coated and noncoated samples, implicating successful antimicrobial activity exhibited by the ZnO microparticle film. In the same confidence interval, mean values for cell viability of *E. coli* and *S. aureus* showed no significant difference, suggesting that differences in cell wall structure did not affect the action mechanism of the ZnO particles in this case. Similar results with successful antimicrobial activity of polymer films with ZnO against *E. coli* and *S. aureus* strains were obtained in various studies [50,51].

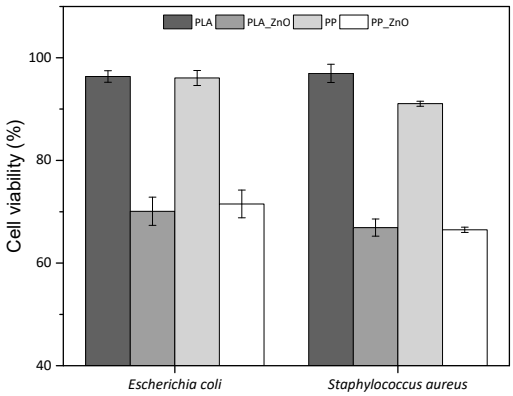


**Figure 23.** Bacteria cell viability after 24 h treatment with coated and noncoated PLA and PP films. There is no significant difference in the antimicrobial activity between *E. coli* and *S. aureus* ($p < 0.05$).

Figure 24 shows the FESEM images of ZnO@PLA and ZnO@PP supports after the antimicrobial assays performed by culturing *E. coli* and *S. aureus* bacteria on both the samples typologies. In this case, the ZnO coating was still present, as further indicated by the presence of diffraction peaks belonging to ZnO (Figure 12c,d) as well as by the EDX compositional analyses reported in Table 1, which confirm the detection of Zn element in high amounts (around 15 at.%) for both PLA and PP supports. However, the morphology of the microparticles has changed from a flower-like structure to a more compact and round-shaped one. EDX data shown in Table 1 also underline the presence of other elements (Na, Ca, P, etc.) due to the interaction of the considered samples with the medium for bacteria culture.

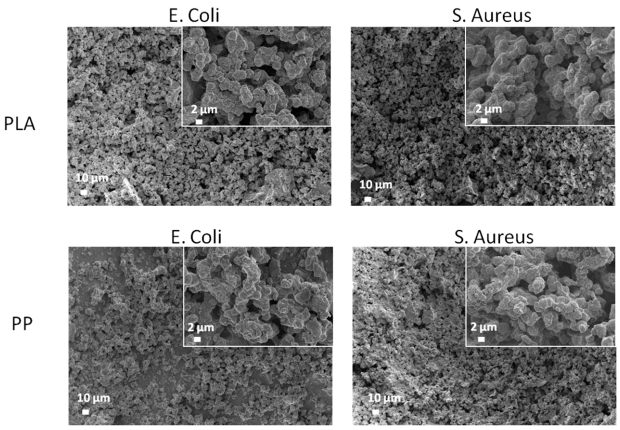


**Figure 24.** FESEM images of ZnO-coated PLA (top panels) and PP (bottom panels) samples after the antimicrobial assays performed by culturing *E. coli* (left panels) and *S. aureus* bacteria (right panels).

**Table 1.** Chemical composition at the surface of ZnO-coated PLA and PP supports after antimicrobial assays.

| Element | *E. coli* | | *S. aureus* | |
|---|---|---|---|---|
| | **PLA/ZnO, at.%** | **PP/ZnO, at.%** | **PLA/ZnO, at.%** | **PP/ZnO, at.%** |
| C | 28.89 | 51.08 | 35.93 | 29.94 |
| N | 4.33 | – | – | 4.70 |
| O | 38.17 | 30.23 | 37.49 | 38.85 |
| Na | 7.69 | 4.97 | 7.21 | 7.36 |
| P | 3.17 | 2.12 | 2.86 | 2.75 |
| Cl | 1.14 | 0.69 | 1.26 | 0.79 |
| K | 0.92 | 0.91 | 0.92 | 0.74 |
| S | – | 0.13 | – | – |
| Ca | – | 0.35 | – | – |
| Zn | 15.69 | 9.52 | 14.33 | 14.87 |
| Total. | 100.00 | 100.00 | 100.00 | 100.00 |

## 4. Conclusions

ZnO coatings were deposited on PLA and PP films by the doctor-blade technique. The ZnO functional layer was obtained starting from high-surface-area, flower-like ZnO microparticles prepared following a simple hydrothermal route. The resulting ZnO@PLA and ZnO@PP samples were studied from the morphological, compositional and structural standpoint. The biodegradation behaviour was investigated by considering the interaction of the considered samples with simulated body fluid and artificial urine solution for prolonged soaking times. Finally, the antimicrobial behaviour was studied as well against *S. aureus* and *E. coli*. It turned out that adhesion of the ZnO coating was better on PLA supports than on PP. The addition of the ZnO functional layer did not negatively influence the mechanical and thermal properties of both PLA and PP supports. Meanwhile, the surface wetting properties of the polymers changed after ZnO deposition and moved from the hydrophobic to the hydrophilic range. When both the samples typologies were soaked into SBF, ZnO dissolution was only partial and independent of the polymer substrate type. It was also found that both PP and PLA substrates prevent the precipitation/formation of phosphate compounds. The presence of the ZnO coating, in contrast, promoted the formation of phosphate compounds. On the contrary, a strong degradation of the ZnO functional coating was observed when the samples were soaked in artificial urine solution. After 21 days, all characterization results pointed out a complete degradation of the ZnO layer due to the acidic pH conditions of the artificial urine environment. The formation of precipitates/encrustations was observed mostly for PP and ZnO@PP, while it was limited on PLA and ZnO@PLA. The composition of the formed compounds was confirmed by compositional analysis and IR spectroscopy. The antimicrobial tests highlighted a good antibacterial activity against both the considered families of bacteria only in the presence of the functional ZnO coating. It is also worth mentioning that the ZnO coating was not affected by the medium for bacteria culture as it was still present after the bacteria culture.

**Author Contributions:** Conceptualization, V.C. and D.M.D.; investigation, C.V., M.L., M.B., E.L., and L.L.; data curation, C.V., M.L., and M.B.; writing—original draft preparation, C.V. and M.L.; writing—review and editing, all authors; supervision, M.L., V.C., and D.M.D. All authors have read and agreed to the published version of the manuscript.

**Funding:** This publication has emanated from research conducted with the financial support of Athlone Institute of Technology under the Presidents Seed Fund, Universidade de Caxias do Sul, grant number CAPES (PDSE - 88881.187620/2018-01) and European Network of Multidisciplinary Research to Improve the Urinary Stents (ENIUS) COST Action CA16217.

**Conflicts of Interest:** The authors declare no conflict of interest.

## References


1. Lam, J.S.; Gupta, M. Update on ureteral stents. *Urology* **2004**, *64*, 9–15. [CrossRef] [PubMed]
2. Yang, L.; Whiteside, S.; Cadieux, P.A.; Denstedt, J.D. Ureteral stent technology: Drug-eluting stents and stent coatings. *Asian J. Urol.* **2015**, *2*, 194–201. [CrossRef] [PubMed]
3. Kim, H.-H.; Kim, K.-W.; Choi, Y.H.; Lee, S.B.; Baba, Y. Numerical analysis of urine flow with multiple sizes of double-j stents. *Appl. Sci.* **2020**, *10*, 4291. [CrossRef]
4. Abdelaziz, A.Y.; Fouda, W.B.; Mosharafa, A.A.; Abelrasoul, M.A.; Fayyad, A.; Fawzi, K. Forgotten ureteral stents: Risk factors, complications and management. *Afr. J. Urol.* **2018**, *24*, 28–33. [CrossRef]
5. Liu, S.; Luo, G.; Sun, B.; Lu, J.; Zu, Q.; Yang, S.; Zhang, X.; Dong, J. Early removal of double-j stents decreases urinary tract infections in living donor renal transplantation: A prospective, randomized clinical trial. *Transplant. Proc.* **2017**, *49*, 297–302. [CrossRef]
6. Ahallal, Y.; Khallouk, A.; Fassi, M.J.E.; Farih, M.H. Risk factor analysis and management of ureteral double-j stent complications. *Rev. Urol.* **2010**, *12*, e147–e151. [CrossRef]
7. Forbes, C.; Scotland, K.B.; Lange, D.; Chew, B.H. Innovations in ureteral stent technology. *Urol. Clin.* **2019**, *46*, 245–255. [CrossRef]
8. Singha, P.; Locklin, J.; Handa, H. A review of the recent advances in antimicrobial coatings for urinary catheters. *Acta Biomater.* **2017**, *50*, 20–40. [CrossRef]
9. Cauda, F.; Cauda, V.; Fiori, C.; Onida, B.; Garrone, E. Heparin coating on ureteral double j stents prevents encrustations: An in vivo case study. *J. Endourol.* **2008**, *22*, 465–472. [CrossRef]
10. Mosayyebi, A.; Vijayakumar, A.; Yue, Q.Y.; Bres-Niewada, E.; Manes, C.; Carugo, D.; Somani, B.K. Engineering solutions to ureteral stents: Material, coating and design. *Cent. Eur. J. Urol.* **2017**, *70*, 270–274. [CrossRef]
11. Cauda, F.; Cauda, V.; Fiori, C. Coated ureteral stent. In *Biomaterials and Tissue Engineering in Urology*; Denstedt, J., Atala, A., Eds.; Woodhead Publishing Ltd.: London, UK, 2009; pp. 134–156.
12. Laurenti, M.; Grochowicz, M.; Dragoni, E.; Carofiglio, M.; Limongi, T.; Cauda, V. Biodegradable and drug-eluting inorganic composites based on mesoporous zinc oxide for urinary stent applications. *Materials* **2020**, *13*, 3821. [CrossRef] [PubMed]
13. Dave, R.N.; Joshi, H.M.; Venugopalan, V.P. Novel biocatalytic polymer-based antimicrobial coatings as potential ureteral biomaterial: Preparation and in vitro performance evaluation. *Antimicrob. Agents Chemother.* **2011**, *55*, 845–853. [CrossRef] [PubMed]
14. Venkatesh, C.; Clear, O.; Major, I.; Lyons, J.G.; Devine, D.M. Faster release of lumen-loaded drugs than matrix-loaded equivalent in polylactic acid/halloysite nanotube. *Materials* **2019**, *12*, 1830. [CrossRef] [PubMed]
15. Turalija, M.; Bischof, S.; Budimir, A.; Gaan, S. Antimicrobial PLA films from environment friendly additives. *Compos. Part B Eng.* **2016**, *102*, 94–99. [CrossRef]
16. Zhang, H.; Hortal, M.; Jorda Beneyto, M.; Rosa, E.; Lara, M.; Lorente, I. ZnO-PLA nanocomposite coated paper for antimicrobial packaging application. *LWT-Food Sci. Technol.* **2016**, *78*, 250–257. [CrossRef]
17. De Silva, R.T.; Pasbakhsh, P.; Lee, S.M.; Kit, A.Y. Zno deposited/encapsulated halloysite–poly(lactic acid) (PLA) nanocomposites for high performance packaging films with improved mechanical and antimicrobial properties. *Appl. Clay Sci.* **2015**, *111*, 10–20. [CrossRef]
18. Pantani, R.; Gorrasi, G.; Vigliotta, G.; Murariu, M.; Dubois, P. PLA-ZnO nanocomposite films: Water vapor barrier properties and specific end-use characteristics. *Eur. Polym. J.* **2013**, *49*, 3471–3482. [CrossRef]
19. Marra, A.; Silvestre, C.; Duraccio, D.; Cimmino, S. Polylactic acid/zinc oxide biocomposite films for food packaging application. *Int. J. Biol. Macromol.* **2016**, *88*, 254–262. [CrossRef]
20. Anžlovar, A.; Kržan, A.; Žagar, E. Degradation of PLA/ZnO and PHBV/ZnO composites prepared by melt processing. *Arab. J. Chem.* **2018**, *11*, 343–352. [CrossRef]
21. Maddah, H.A. Polypropylene as a promising plastic: A review. *Am. J. Polym. Sci.* **2016**, *6*, 1–11. [CrossRef]
22. Okuyucu, S.; Gorur, H.; Oksuz, H.; Akoglu, E. Endoscopic dacryocystorhinostomy with silicone, polypropylene, and t-tube stents; randomized controlled trial of efficacy and safety. *Am. J. Rhinol. Allergy* **2015**, *29*, 63–68. [CrossRef] [PubMed]
23. Viswanatha, B.; Vijayashree, M.S. Silicone stenting and polypropylene stenting in endoscopic dacryocystorhinostomy: A prospective comparative study. *Res. Otolaryngol.* **2015**, *4*, 49–53. [CrossRef]

24. Mitsuoka, M.; Hayashi, A.; Takamori, S.; Tayama, K.; Shirouzu, K. Experimental study of the histocompatibility of covered expandable metallic stents in the trachea. *Chest* **1998**, *114*, 110–114. [CrossRef] [PubMed]
25. Yuan, T.; Zheng, R.; Yu, J.; Edmonds, L.; Wu, W.; Cao, J.; Gao, F.; Zhu, Y.; Cheng, Y.; Cui, W. Fabrication and evaluation of polymer-based esophageal stents for benign esophagus stricture insertion. *RSC Adv.* **2016**, *6*, 16891–16898. [CrossRef]
26. Zhao, H.; Li, R.K.Y. A study on the photo-degradation of zinc oxide (ZnO) filled polypropylene nanocomposites. *Polymer* **2006**, *47*, 3207–3217. [CrossRef]
27. Jakubiak, S.; Tomaszewska, J.; Jackiewicz, A.; Michalski, J.; Kurzydłowski, K.J. Polypropylene–zinc oxide nanorod hybrid material for applications in separation processes. *Chem. Process Eng.* **2016**, *37*, 393–403. [CrossRef]
28. Bojarska, M.; Nowak, B.; Skowroński, J.; Piątkiewicz, W.; Gradoń, L. Growth of ZnO nanowires on polypropylene membrane surface—characterization and reactivity. *Appl. Surf. Sci.* **2017**, *391*, 457–467. [CrossRef]
29. Mirzaei, H.; Darroudi, M. Zinc oxide nanoparticles: Biological synthesis and biomedical applications. *Ceram. Int.* **2017**, *43*, 907–914. [CrossRef]
30. Garino, N.; Sanvitale, P.; Dumontel, B.; Laurenti, M.; Colilla, M.; Izquierdo-Barba, I.; Cauda, V.; Vallet-Regì, M. Zinc oxide nanocrystals as a nanoantibiotic and osteoinductive agent. *RSC Adv.* **2019**, *9*, 11312–11321. [CrossRef]
31. Król, A.; Pomastowski, P.; Rafińska, K.; Railean-Plugaru, V.; Buszewski, B. Zinc oxide nanoparticles: Synthesis, antiseptic activity and toxicity mechanism. *Adv. Colloid Interface Sci.* **2017**, *249*, 37–52. [CrossRef]
32. Pasquet, J.; Chevalier, Y.; Pelletier, J.; Couval, E.; Bouvier, D.; Bolzinger, M.-A. The contribution of zinc ions to the antimicrobial activity of zinc oxide. *Colloids Surf. A Physicochem. Eng. Asp.* **2014**, *457*, 263–274. [CrossRef]
33. Dimapilis, E.A.S.; Hsu, C.-S.; Mendoza, R.M.O.; Lu, M.-C. Zinc oxide nanoparticles for water disinfection. *Sustain. Environ. Res.* **2018**, *28*, 47–56. [CrossRef]
34. Racca, L.; Canta, M.; Dumontel, B.; Ancona, A.; Limongi, T.; Garino, N.; Laurenti, M.; Canavese, G.; Cauda, V. Zinc oxide nanostructures in biomedicine. In *Smart Nanoparticles for Biomedicine*; Ciofani, G., Ed.; Elsevier: Amsterdam, The Netherlands, 2018; pp. 171–187.
35. Pugliese, D.; Bella, F.; Cauda, V.; Lamberti, A.; Sacco, A.; Tresso, E.; Bianco, S. A chemometric approach for the sensitization procedure of ZnO flowerlike microstructures for dye-sensitized solar cells. *ACS Appl. Mater. Interfaces* **2013**, *5*, 11288–11295. [CrossRef] [PubMed]
36. Cauda, V.; Stassi, S.; Lamberti, A.; Morello, M.; Fabrizio Pirri, C.; Canavese, G. Leveraging ZnO morphologies in piezoelectric composites for mechanical energy harvesting. *Nano Energy* **2015**, *18*, 212–221. [CrossRef]
37. Shin, J.; Liu, X.; Chikthimmah, N.; Lee, Y.S. Polymer surface modification using uv treatment for attachment of natamycin and the potential applications for conventional food cling wrap (ldpe). *Appl. Surf. Sci.* **2016**, *386*, 276–284. [CrossRef]
38. Socrates, G. *Infrared and Raman Characteristic Group Frequencies: Tables and Charts*; John Wiley & Sons: Chichester, UK, 2004.
39. Kokubo, T.; Takadama, H. How useful is SBF in predicting in vivo bone bioactivity? *Biomaterials* **2006**, *27*, 2907–2915. [CrossRef]
40. Sarangapani, S.; Cavedon, K.; Gage, D. An improved model for bacterial encrustation studies. *J. Biomed. Mater. Res.* **1995**, *29*, 1185–1191. [CrossRef]
41. Kruenate, J.; Tongpool, R.; Panyathanmaporn, T.; Kongrat, P. Optical and mechanical properties of polypropylene modified by metal oxides. *Surf. Interface Anal.* **2004**, *36*, 1044–1047. [CrossRef]
42. Jayaramudu, J.; Das, K.; Sonakshi, M.; Siva Mohan Reddy, G.; Aderibigbe, B.; Sadiku, R.; Sinha Ray, S. Structure and properties of highly toughened biodegradable polylactide/zno biocomposite films. *Int. J. Biol. Macromol.* **2014**, *64*, 428–434. [CrossRef]
43. Tang, Z.; Fan, F.; Chu, Z.; Fan, C.; Qin, Y. Barrier properties and characterizations of poly(lactic acid)/ZnO nanocomposites. *Molecules* **2020**, *25*, 1310. [CrossRef]
44. Laurenti, M.; Lamberti, A.; Genchi, G.G.; Roppolo, I.; Canavese, G.; Vitale-Brovarone, C.; Ciofani, G.; Cauda, V. Graphene oxide finely tunes the bioactivity and drug delivery of mesoporous ZnO scaffolds. *ACS Appl. Mater. Interfaces* **2019**, *11*, 449–456. [CrossRef] [PubMed]
45. Laurenti, M.; Cauda, V. Gentamicin-releasing mesoporous ZnO structures. *Materials (Basel)* **2018**, *11*, 314. [CrossRef] [PubMed]
46. Salma, K.; Borodajenko, N.; Plata, A.; Berzina-Cimdina, L.; Stunda, A. Fourier transform infrared spectra of technologically modified calcium phosphates. In Proceedings of the 14th Nordic-Baltic Conference on Biomedical Engineering and Medical Physics, Riga, Latvia, 16–20 June 2008.

47. Richardson, J.J.; Lange, F.F. Controlling low temperature aqueous synthesis of ZnO. 1. Thermodynamic analysis. *Cryst. Growth Des.* **2009**, *9*, 2570–2575. [CrossRef]
48. Sedłak, A.; Janusz, W. Specific adsorption of carbonate ions at the zinc oxide/electrolyte solution interface. *Physicochem. Probl. Miner. Process.* **2008**, *42*, 57–66.
49. Haleblian, G.; Kijvikai, K.; Rosette, J.d.l.; Preminger, G. Ureteral stenting and urinary stone management: A systematic review. *J. Urol.* **2008**, *179*, 424–430. [CrossRef]
50. Mizielińska, M.; Kowalska, U.; Jarosz, M.; Sumińska, P.; Landercy, N.; Duquesne, E. The effect of UV aging on antimicrobial and mechanical properties of PLA films with incorporated zinc oxide nanoparticles. *Int. J. Environ. Res. Public Health* **2018**, *15*, 794. [CrossRef]
51. Mania, S.; Cieślik, M.; Konzorski, M.; Święcikowski, P.; Nelson, A.; Banach, A.; Tylingo, R.T. The synergistic microbiological effects of industrial produced packaging polyethylene films incorporated with zinc nanoparticles. *Polymers* **2020**, *12*, 1198. [CrossRef]